PAPER NUMBER

124

CORROSION 91

The NACE Annual Conference and Corrosion Show

March 11-15, 1991 • Cincinnati Convention Center • Cincinnati, Ohio

CORROSION PERFORMANCE OF EPOXY-COATED REINFORCING STEEL IN MARINE SUBSTRUCTURE SERVICE

A.A. Sagues, H. M. Perez-Duran
Department of Civil Engineering and Mechanics
University of South Florida
Tampa, Florida 33620

R.G. Powers
Materials Office
Florida Department of Transportation
Gainesville, Florida 32602

ABSTRACT

Corrosion of marine bridge substructures using concrete with epoxy-coated reinforcing steel (ECR) has been observed in Florida Keys bridges. Experiments have been conducted to determine the extent of corrosion and associated macrocell action in concrete that might develop in ECR that contained surface defects and was subject to corrosion before placement in concrete. Instrumented columns have been used to measure the extent of macrocell action and determine the cathodic polarization behavior of ECR segments. A simplified quantitative model has been formulated to predict the macrocell current distribution along idealized substructure columns, as a function of concrete resistivity, column length and ECR surface condition.
Keywords: epoxy, coating, damage, corrosion, disbondment, delamination, concrete, chloride, bridges, macrocells, cathodic, polarization, model, calculations.

INTRODUCTION

Epoxy-coated rebar (ECR) has been in frequent use in the United States since the mid-1970's [1]. The main highway application is in the decks of bridges subject to deicing salts, but the product has also been used as reinforcement in the substructure of marine bridges. The epoxy coating is applied to the surface of freshly blasted steel at high temperature [2]. The finished coating must comply with ASTM A-775 or similar specifications. Initial research generally addressing bridge deck construction [3,4] showed that epoxy-coated reinforcing steel would be expected to perform significantly better than uncoated reinforcement. With the possible exception of an initial experimental product, the performance to date in highway bridge decks has been

reported to be successful [1,5]. In contrast, incidents of severe corrosion of epoxy-coated rebar have been recorded in the substructure of four major bridges in the Florida Keys after six to ten years of service. The damage tended to affect portions of the substructure in the splash and evaporation zone, where high chloride concentrations (as high as 23 pounds per cubic yard (pcy) or 13.7 Kg/m^3) can build up at the rebar depth after a few years of service. Corrosion proceeded underneath the epoxy coating, with black corrosion products thinly spread or forming at pits, and frequent accumulation of low pH, chloride-rich liquid. The coating material itself was visually unaffected and had a thickness consistent with the initial specifications. There is no conclusive evidence of deviation from the product specifications at the time of coating application. Additional information on the damage morphology and service conditions has been provided in References [6] to [10].

Research aimed at identifying the causes of the deterioration observed in the Florida Keys has addressed the influence of mechanical fabrication [8,11], and possible coating delamination mechanisms before and after placement of the epoxy-coated rebar in concrete [9,10]. The latter investigations consisted of laboratory experiments using model liquid solutions and epoxy-coated bars that met current specifications. Both as-received and intentionally surface-damaged bars were used. It was observed that one-month exposure to calcium hydroxide-sodium chloride mixed solutions under anodic polarization conditions caused both delamination around defects, pits with black corrosion products, and accumulation of low pH liquid between the coating and the underlying metal [9]. The similarity between the anodic laboratory behavior and the field corrosion morphology suggested that the damage at the bridges may have taken place at the anodic end of corrosion macrocells, which could be active in the marine substructures [12,13,14]. Possible deterioration of the material at the construction yard, before placement in concrete, due to seawater spray was also addressed in the experiments. It was seen that exposure to neutral sodium chloride only solutions under open circuit conditions could cause significant disbondment around existing or introduced coating imperfections. This disbondment revealed bright metal underneath, presenting the characteristics of ordinary cathodic disbondment as observed underneath certain organic coatings [15]. Specimens preexposed to simple sodium chloride solutions tended to show aggravated deterioration (compared with specimens that were not preexposed) when tested afterwards under anodic polarization in a calcium hydroxide-sodium chloride solution [16].

The results described above suggest that electrochemical disbondment of the coating due to seawater spray, and subsequent macrocell action during service in the bridge substructure may have been strong contributing factors to the deterioration eventually observed in the field. To test this possibility, experiments and quantitative assessments of the corrosion conditions prevalent in Florida's marine substructures are in progress. This paper presents a summary of the ongoing effort and its initial results.

EXPERIMENTAL INVESTIGATION

The purpose of this work was to determine the extent of corrosion and associated macrocell action that might develop in epoxy-coated reinforcing steel (containing a controlled amount of surface defects) in concrete under simulated marine substructure conditions. In addition, it was desired to establish whether disbondment associated with prior saltwater exposure of the coated rebar would significantly affect corrosion severity once the rebar was placed in service.

The experimental approach consisted of preparing concrete columns that contained multiple rebar segments placed at various levels, and placing the bottom of the column in contact with water containing sodium chloride. As water is transported upward by capillary action, it reaches drier regions where it evaporates and leaves behind dissolved salts. A chloride accumulation zone is thus created some distance above the waterline, resembling the distribution pattern present in substructure members of a marine bridge. There is also an associated moisture gradient (and consequently also an electrical resistivity gradient) along the column following the general pattern experienced in the field [8,12,13]. External electrical contacts permit measuring macrocell currents, concrete resistivity, and polarization behavior as a function of exposure time, thus providing ongoing information to supplement the results of final specimen autopsy.

The columns used in this investigation were constructed as shown in Figure 1. Each column was 48 inches (1.2 m) tall, 12 inches (0.3 m) wide and approximately 4 inches (0.1 m) thick. Eleven segments of #7 ECR were placed horizontally at regular vertical intervals. The effective length of each segment was approximately 8.5 inches (0.22 m). The bars were slightly off-center and facing an inset in the casting form, to allow for reduced concrete cover on one side. Activated titanium reference electrodes were embedded just below each rebar segment to permit easy polarization measurements. The ends of the bars and all internal electrical connections were covered by metallographic epoxide compound to prevent unwanted galvanic action. All connection leads were routed to the top of the column toward a connection box. The switches connecting together all the rebar segments were normally in the closed position. Longitudinal fiberglass-reinforced plastic bars were embedded in the columns to provide additional strength without interfering with the corrosion behavior.

The ECR was obtained from a regular production run of a major supplier to the Florida Department of Transportation (FDOT). Visual examination of the material revealed it to be unblemished, corresponding to the highest FDOT appearance rating. The thickness of the coating, as determined by a magnetic gage, complied with the guidelines specified in ASTM A-775. Controlled surface damage was introduced on each rebar segment by making file marks at even intervals at the center of deformation ribs and also at the two longitudinal deformations. The file markings exposed bare metal in small regions, roughly rectangular and typically 2mm by 4 mm in size. Each 0.22 m long segment of bar included nominally 32 file markings. The average amount of metal surface exposed per bar corresponded to approximately 2% of the nominal bar surface (estimated at 32 square inches per linear foot (677 cm^2/m) [17]).

The concrete used to build the columns had a w/c ratio of 0.45 , Type I cement with a cement factor of 611 pcy, and coarse and fine aggregates normally used in Florida substructure applications. To accelerate the test, the concrete mix for the lower 10 inches (0.25 m) of the columns had an added 20 pcy (11.9 Kg/m^3) of chlorides, by including the appropriate amount of NaCl. A removable baffle separated the lower part of the column from the rest when pouring the concrete. After moist-curing for 5 days, the columns were exposed to laboratory air for 6 additional days and then put in an exposure tank so that the lower 5 inches (0.125 m) were immersed in water containing 5% NaCl. The rebar segments were interconnected shortly afterward; exposure times are counted from the nominal moment of interconnection.

A total of eight columns was prepared using the procedure described above. Four of those columns included rebar specimens that had undergone the surface marking process but no additional treatment. This first group of columns, numbered 1 through 4, was designated Group

A. The other four columns were built with specimens that had experienced exposure to neutral water with 3.5% NaCl in shallow trays for 30 days. These specimens were then lightly rinsed with fresh water and blotted dry before placement in concrete. This second group of columns (numbered 5 through 8) was designated Group B.

Nominal concrete resistivity measurements were performed by opening all switches between the rebar elements, and circulating a 10 uA, 200 Hz a.c. current (Iac) between the highest and lowest rebar segment. The resulting a.c. potential drop between reference electrodes placed at the different levels was then recorded. The apparent average resistivity, ρ, of the concrete located between any two reference electrodes was then evaluated by

$$\rho = \text{Vac.Acs/d.Iac} \qquad (1)$$

where Vac is the a.c. potential drop between the two electrodes, Acs is the cross-sectional area of the column expressed in cm^2, and d is the vertical distance between electrodes expressed in cm.

The switches between the rebar segments were normally left in the closed (conducting) position. Currents circulating through the closed switches were measured by opening the switches momentarily and inserting a custom-made Zero Resistance Ammeter (ZRA) in the circuit.

The potential of each segment with respect to the surrounding concrete was evaluated by measuring the difference in potential between the segment and the reference electrode immediately below the segment. All the switches between segments were then momentarily opened, and the potential of each internal reference electrode was measured with respect to a Saturated Calomel Electrode (SCE) placed in contact with the liquid at the bottom. This procedure calibrated the internal reference electrodes while avoiding errors due to macrocell-induced IR drops in the concrete.

RESULTS

The ECR specimens prepared for column group B by precorroding in a 3.5% NaCl solution for one month developed open circuit potentials close to -700 mV vs SCE during that exposure. While rust was visible at most of the exposed metal spots after exposure, metal loss was minimal. However, tests with short segments showed that the precorrosion treatment lead to significant disbondment of the coating around the intentionally introduced imperfections. The coating could be easily separated from the metal for a distance of about 5 mm from the edge of the imperfection. This is in agreement with observations of comparable disbondment at open circuit conditions for similar ECR material [9].

Resistivity trends in the assembled columns were documented. Figure 2 exemplifies the results of measurements of apparent concrete resistivity for one of the columns; this behavior was essentially the same for all the other columns. Shortly after beginning the test, the resistivity in most of the portion of the column above water was on the order of 5000 ohm-cm. Lower values were recorded near the submerged zone. The resistivity of the region above water increased with time; after 160 days of exposure the resistivity approached 20,000 ohm-cm at the top of the column.

All columns in group A (rebar segments not pre-corroded) developed consistent macrocell current patterns shortly after initiation of the test. Typical behavior is illustrated in Figure 3 (left), which shows the macrocell currents measured at each of the switches in Column 1 after 3 and 160 days of exposure. The electronic macrocell current flowed at all levels from the lower to the upper element. The maximum measured current took place usually at switch nine, located between the two lower elements in high-chloride concrete and the rest of the column.

The net current Is_i sinking in (or flowing from) rebar segment i can be calculated by computing the current differences from consecutive segments (segment 1 is at the top):

$$Is_i = Im_i - Im_{(i-1)} \quad (1 < i < 11)$$

$$Is_1 = Im_1$$

$$Is_{11} = -Im_{10} \qquad (2)$$

Where Im_i is the macrocell current measured at switch level i (level 1 is at the top).

Figure 3 (right side) shows the result of applying Eq.(1) to the data shown in the left side. The two lower segments were net anodes, while the rest of the segments were net cathodes. That pattern was generally maintained through the entire test period. While the magnitude of the macrocell currents tended to fluctuate with time, there was an increasing trend as test time progressed (see below). This increase is reflected in the values of the total and net currents displayed in Figure 3 for early and late exposure times.

The columns in Group B (precorroded rebar segments) showed similar behavior as Group A when active behavior was observed. Column 6 in Group B showed the highest macrocell currents measured so far in this study. However, during the exposure period to date (117 days), only two of the columns in Group B had developed active macrocell patterns. Figure 4 illustrates the development and relative intensity of the macrocell action in both groups of columns, by displaying the macrocell current at switch #9 for each column as a function of exposure time.

The potential measurements gave results that were related to the extent of macrocell activity observed; more negative potentials were measured at segments in columns with the larger macrocell currents. Figure 5 shows the segment potentials measured in both column groups at about the same exposure times, as a function of the log of Is, for segments with predominantly cathodic behavior. The potentials within a given column tended to span a relatively small range, typically less than 100 mV.

DISCUSSION

The resistivity measurements reported in Figure 2 are only approximate averages, since the concrete resistivity is expected to vary to some degree across each horizontal cross section of the column. Further error results from the current being sent through the top and bottom rebar segments, which creates a deviation from ideal parallel current flow. The value reported for the lowest column portion sampled should be considered as a nominal value, since this portion is partially in contact with salt water, which acts as a shunt to the measuring current. Keeping in mind the approximate nature of the measurements, they nevertheless reflect the progressive curing

and drying of the portion of the column above water. The values fall within the range normally observed in concrete with varying amounts of moisture [18-20]. The measured values approach also the field conditions of interest. Preliminary measurements performed at marine Florida bridges have shown concrete resistivities (near the surface) in the 3,000 to 10,000 ohm-cm range, in the substructure region where corrosion tends to be severe [16].

The corrosion macrocell currents developed in the expected direction. Predominantly anodic behavior was observed in the lower two elements, in which the exposed metal was in contact with high-chloride concrete and therefore expected to be active. Net cathodic behavior was evident in the upper region. In that region the exposed metal is in contact with low-chloride concrete that promotes passivity, and the low moisture content is conducive to easier oxygen transport to the metal surface, thus facilitating the cathodic reaction [22].

The magnitude of the largest macrocell currents was on the order of tens of microamperes. As shown in Figure 4, the highest values were recorded for one of the columns (#8, Group B) containing precorroded ECR segments, but considerable variation was observed within specimens from each group. The differences reflect variations in the extent of passivity loss experienced during the relatively short test times accumulated to date. More uniform behavior is expected as chloride concentration at the surface of the lower rebars continues to build up above the initial loading levels.

Comparisons of the cathodic behavior of both groups of columns may be made, even at this early stage of testing, by taking into consideration the extent of the net cathodic currents and corresponding potentials observed. The rebar segments in the upper portion of the columns are likely to remain in chloride-free concrete over long periods, retaining a relatively stable environment. Variations from column to column in the anodic reaction rate at the lower rebar segments are reflected in the polarization of the cathodic processes in the upper part of the columns. This results in each column within a given group having its own range of potentials and sink currents at the predominantly cathodic segments. Figure 5 combines the polarization information from both groups of columns, obtained at about the same exposure time.

The polarization data from group B includes potentials that were less negative than in group A. This indicates that active corrosion was developed to a lesser extent than in the group A columns at the time the measurements were taken. The data for the group B columns provides an opportunity to examine the polarization behavior over a wide potential range. At the low current levels there is an apparent Tafel region, with a slope of about 100 to 150 mV/decade, which is comparable with values commonly reported in the literature for oxygen reduction on steel [23]. At higher currents the curves for both groups A and B bend downward, suggesting the onset of a diffusion-limited regime. The current values shown in Figure 5 may be reduced to apparent current densities by dividing the current by the nominal area of metal exposed per bar segment during the specimen preparation procedure (typically 2.5 cm^2, about the same for both groups of columns). The data in Figure 5 suggest therefore that precorroded segments developed a distinctly larger apparent current density, at any given cathodic overpotential, than untreated segments.

One possible cause for increased apparent current density in precorroded segments is the coating disbondment developed during the precorrosion procedure. If after placement in concrete electrolyte penetrates underneath the disbonded coating, then some metal surface becomes available for cathodic reactions in addition to the amount initially exposed. The magnitude of the

reaction at this extra surface could depend on many factors, including the thickness of the electrolyte layer present in the crevice below the disbonded coating, the resistivity of that electrolyte, and the polarization characteristics of the cathodic reaction inside the crevice. Simplified quantitative treatments to predict the extent of the resulting reaction have been developed [24], but not enough is known at this time of the conditions in this system to conduct meaningful calculations. Another source of increased cathodic action in precorroded segments may be semiconducting corrosion products present at the spots where surface damage was introduced, which were subsequently exposed to the NaCl solution. These corrosion products may increase the effective surface area available for the cathodic reaction, thus increasing its overall rate [25].

A quantitative model of the corrosion conditions in the column is desirable to evaluate the impact of the service conditions on corrosion severity. The cathodic/anodic current distribution in the column was modelled by accounting for the polarization behavior of the cathodic and anodic reactions, and the electrical resistance of the intervening concrete. The test specimen configuration used here is suitable for a treatment in which the column is divided into a stack of discrete elements. Figure 6 shows an idealized column with interconnected elements, and a large-signal electrical equivalent circuit. Elements E_1 to E_9 are current-dependent voltage sources representing the potential difference across the metal-concrete interface of the net cathodic regions. E_{10} and E_{11} correspond to the net anodic regions. For simplification, purely cathodic and purely anodic behavior respectively was assumed for those regions. On first approximation, the reactions were considered to be subject only to activation polarization so that for rebar segment $\underline{i}$:

$$E_i = Eoc - bc \log(|Is_i| / Ioc) \qquad (3)$$

if the segment is a cathode, or

$$E_i = Eoa + ba \log(|Is_i| / Ioa) \qquad (4)$$

if the segment is an anode.

The magnitudes bc and ba are the Tafel constants for the cathodic and the anodic processes respectively. Ioc and Ioa are the exchange currents for each process respectively. It was assumed that all cathodic rebar segments within a column have the same amount of effective surface area Ac available for electrochemical reactions, so that Ioc = ioc.Ac, where ioc is the exchange current density for the cathodic process. Likewise, all anodic segments were assumed to have an equal effective area Aa (not necessarily equal to Ac, see below) and an exchange current density ioa. Eoc and Eoa are the unpolarized cathode and anode potentials respectively; the potentials Ei were assumed to be separated enough from the unpolarized values that back reactions could be considered to be negligible.

The effective resistance of the concrete joining consecutive segments $\underline{i}$ and $\underline{i+1}$ was approximated by $Rc_i = \rho_i.d/Acs$ (see Eq.(1)), where ρ_i is the resistivity of the concrete between the two segments. The current through each of the Rc_i elements in the circuit of Figure 6 can be expressed as a function of the Is_i values by Kirchoff's law. This permits expressing the corresponding potential drops across the resistors also in terms of Is_i values.

Independent equations were formulated establishing a zero potential sum for each one of the 10 closed loops in the ladder circuit in Figure 6. An additional equation was provided by the requirement that the sum of all the cathodic currents needs to be equal to the sum of all the anodic currents. The resulting system of eleven equations can be solved to obtain the eleven values of Is, using as input the resistivity profile of the column, and the polarization parameters of the cathodic and anodic reaction.

Ten of the equations in the system involve logarithmic terms in a manner that prevents analytical solution. Instead, the equations were formulated for numerical solution in a commercial mathematical software package (Mathcad). Numerical tolerance parameters and seed solution values required by the program were varied in a test case to verify reproducibility of the solution output.

Figure 7 shows the results of applying the model to the experimental column conditions. The resistivity input was chosen to replicate the resistivity profile for 160 days of exposure shown in Figure 2. Nominal values for Eoc, Ioc and bc were obtained for both groups of columns by using the data in Figure 5 and approximating the polarization curves by straight lines. The resulting nominal cathodic polarization parameters assumed were Eoc=30 mV (vs SCE), bc=188 mV/decade, Ioc=10^{-8} A for column group A, and Ioc=3 10^{-8} A for column group B. The anodic polarization parameters were approximated by noting first the characteristic net current and potentials (typically 10 uA and -450 mV vs SCE respectively) measured at the anodic segments that displayed well-developed active behavior in either column group. That current/potential combination was chosen as a fit point for the anodic polarization curve. A Tafel constant of 60 mV/decade, which is representative of active iron dissolution processes [23] was assumed next. The combination Eoa=-990 mV vs SCE and Ioa=10^{-14} A, which matches the selected operating point and slope, was chosen then to complete the anodic behavior description.

The results of the calculations (Figure 7) replicate several aspects of the experimental behavior which was shown in Figure 3. The calculated cathodic currents reach a maximum when closest to the anodes, decaying slowly at the higher column levels. The calculated system settles at an operating point consistent with the current magnitudes observed experimentally. The calculations predict a maximum of anodic activity at segment #10 (the higher of the two anodes). This results from assuming that both anodic segments have identical polarization behavior; then the segment closest to the cathodes will experience the greatest activity. In the actual columns the anodic behavior will be dictated by the extent of active surface (and its effectiveness if located inside a crevice) present in each segment. This may depend in turn on the extent of chloride buildup at the bar surface, the previous history of the segment, and other factors yet to be identified. As a result, current distribution among the two anodes is complicated and it may vary with time (as illustrated by the behavior of Column 1, Figure 3).

Because of the nominal Tafel slope values chosen, the cathodic reaction exerts most of the control on the extent of the corrosion currents in the model. The difference in cathodic activity between column groups A and B was represented in the model by the choice of cathodic exchange currents differing by a factor of 3. For fully developed anodes, this translates in the different predicted behaviors shown in Figure 7. This predicted change is comparable with the difference in macrocell activity between column 6, group B, and the columns in group A (Figure 4).

The simplified model presented here may be used to explore the effect of substructure service variables in the performance of ECR in the field. The electrical resistance of a column portion is inversely proportional to its cross-section. For a given set of polarization conditions and resistivity distributions, currents will be proportional to the effective surface area of rebar per column unit length, and potential drops along the column will be inversely proportional to its cross-section. Therefore, the ratio P of rebar area per unit length to cross section of the column may be used as a scaling parameter to predict current and potential distributions in other geometrically uniform arrangements.

The laboratory columns have a cross-sectional area of approximately 300 cm^2. The rebar segments used in the column have each a nominal surface area of 149 cm^2, and are separated 10.2 cm apart, corresponding to 14.6 cm^2 of rebar surface for each cm along the column length. The rebar area/unit length to cross section ratio, P, for the laboratory columns is therefore 0.049 cm^{-1}. Substructure columns of the type used in some of the Florida Keys bridges with corroding ECR are round, with a diameter of 3 feet (91.4 cm). There is roughly a 1:1 ratio of surface area of concrete to surface area of reinforcing steel underneath. Those dimensions result in a ratio P = 0.044, close to that of the laboratory specimens (which were designed with that ratio value in mind). Based on that similarity, the model was used to examine the effect of changes in concrete resistivity and column height on the extent of anodic activity to be expected in substructure service. The calculations were based on columns with bars spaced as in the laboratory specimens, using two anodes as before but varying the extent of the cathodic activity by simulating different total column lengths. The cathodes were always spaced 10.2 cm apart, so that longer columns contained proportionally more cathodes. Resistivity was assumed to be constant along the column length. Column lengths, defined as the distance between the highest cathode and the lowest anode, of 3.3 feet (1m), 10 feet (3m) and 20 feet (6m) were simulated. The calculations were performed assuming concrete resistivities of 3,000 ohm-cm and 10,000 ohm-cm. The same polarization behavior used earlier for types A and B columns was assumed in these calculations.

Figure 8 summarizes the result of the calculations, giving the predicted average bar current density (current/total bar surface including both exposed metal and area covered by coating) for the highest of the two anodes as a function of the input parameters. It should be kept in mind that actual localized current densities can be much higher since the defects involve only a small percentage of the total bar surface. On all cases column height was of importance up to about 3m, beyond which the extent of the cathodic reaction became negligible at the highest column levels (small deviations from uniform trends in Figure 8 resulted from the coarse model discretization). Changes in the effective exchange current of the cathodic reaction (the difference between cases A and B) played a more important role than variations on the concrete resistivity. The latter had an even lesser role at the shorter column lengths, where the IR drops are not as significant as in the longer columns.

The absolute value of the average anodic current densities is critical to judging the importance of macrocell phenomena in the development of ECR corrosion in marine substructures. In the laboratory the typical average current densities (for the highest anode) in column group A were about 0.1 uA/cm^2 (note that this current density is calculated as an average over the entire bar segment, including both coated surface and bare metal spots). In column 6, group B, the value was two to three times greater. The calculated values in Figure 8 suggest that average current densities of about 0.2 to 0.3 uA/cm^2 could be reached in typical field structures containing rebar that was treated comparably to the material used in the group B specimens.

Limits between 0.1 and 0.2 uA/cm^2 have been proposed to indicate the threshold of corrosion activity above which deterioration of concrete with ordinary rebar is expected within typical structure service histories [26]. It has been suggested that corrosion currents between 0.2 and 1.0 mA/sq.ft. (approximately 0.2 to 1.0 uA/cm^2), as evaluated from polarization measurements, represent a possibility of corrosion damage within 10 to 15 years of service in systems using conventional rebar [27]. At present there is no information available to determine whether similar levels of average corrosion activity would result in earlier observations of corrosion damage when ECR is used. However, the low adherence between ECR and the surrounding concrete, and the greater likelihood of corrosion localization at surface defects in ECR may act adversely in reducing the corrosion threshold for mechanical damage. In this context, it should be recalled that the ECR corrosion observed in the field was characterized by severe pitting, presumably aggravating the local stress buildup. These issues need to be investigated.

The surface condition used in the test specimens represented a substantial level of damage (about 2%). That amount of exposed metal might have been originally present in the structures under consideration, since suggested jobsite practice at the time permitted that level of unpatched damage [17]. As indicated in the introduction, it is possible that significant disbondment may have also developed, either by mechanical fabrication or electrochemical action. The apparent increase in cathodic activity observed in the precorroded specimens suggests that a comparable process could have created efficient cathodes at the ECR in the affected bridges. Experiments are in progress to further assess the extent of cathodic reaction in disbonded ECR.

The behavior at the anodes is difficult to characterize because of the localized nature of the reaction, at least during the early stages of deterioration. As indicated earlier, once enough active area is developed the corrosion process is likely to be under cathodic control. The model used a simple, relatively large cathodic Tafel slope to simulate that condition. A more accurate approach would be to simulate a diffusion-limited regime at the high cathodic current end.

The results and discussion presented above reflect initial findings of an investigation in progress. Additional results and a more detailed analysis will be given in a future presentation.

CONCLUSIONS

1. Corrosion macrocell currents took place in reinforced concrete laboratory columns built with epoxy coated rebar containing about 2% surface defects. The cathodic portion of the columns tended to show greater ability to deliver current if the damaged rebar was subject to prior corrosion in an NaCl solution.

2. A simplified quantitative model of the column was formulated using as input the resistivity distribution of the concrete and polarization parameters for the anodic and cathodic reactions. The model reproduced the main features of the macrocell current pattern observed in the laboratory.

3. Using scaling criteria based on the proportion of rebar to concrete, the model was applied to evaluate average corrosion rates in a field situation. Average corrosion current densities on the order of 0.2 to 0.3 uA/cm^2 were calculated for the anodic regions of a typical substructure member subject to extended macrocell action. The effect of those average current densities in a system using epoxy-coated rebar (as compared to ordinary rebar) need to be investigated.

ACKNOWLEDGMENT

This investigation was supported in cooperation by the Florida Department of Transportation and the U.S. Department of Transportation. The opinions, findings and conclusions expressed in this document are those of the authors and not necessarily those of the State of Florida Department of Transportation or the U.S. Department of Transportation.

REFERENCES

1. Gustafson, D., Epoxy Update. Civil Engineering, 1988 (October), Vol. 58, p.38.

2. Salparanta, L., Epoxy Coated Concrete Reinforcements, Research Report 525, (ISBN 951-38-3094-2), Technical Centre of Finland, Espoo, March 1988.

3. Virmani, Y., Clear, K. and Pasko, T., Time to Corrosion of Reinforcing Steel in Concrete Slabs, Vol.5:Calcium Nitrite Admixture and Epoxy-Coated Reinforcing Bars as Corrosion Protection Systems, Report No. FHWA/RD-83/012, National Technical Information Service, Springfield, Virginia, 1983.

4. Clear, K. and Virmani, Y., Corrosion of Nonspecification Epoxy-Coated Rebars in Salty Concrete, Public Roads, 1983 (June), Vol. 47, p.1.

5. Malasheskie, G., Maurer, D., Mellot, D., and Arellano, J., "Bridge Deck Protective Systems", Report FHWA-PA-88-001+85-17, (prepared by Pennsylvania Dept. of Transportation), July 1988, available from National Tech. Info. Center, Springfield, VA.

6. Kessler, R. and Powers, R. Interim Report, Corrosion Evaluation of Substructure, Long Key Bridge, Corrosion Report No. 87-9A, Materials Office, Florida Department of Transportation, Gainesville, 1987.

7. Powers, R. Corrosion of Epoxy Coated Rebar, Keys Segmental Bridges, Corrosion Report No. 88-8A, Florida Dept. of Transportation, Gainesville, Florida, 1987.

8. Zayed, A., Sagues, A. and Powers, R. Corrosion of Epoxy Coated Reinforcing Steel in Concrete, Paper No. 379, Corrosion/89, National Association of Corrosion Engineers, Houston, 1989.

9. Sagues, A. and Powers, R. Effect of Concrete Environment on the Corrosion Performance of Epoxy-Coated Reinforcing Steel, Paper No. 311, Corrosion/90, National Association of Corrosion Engineers, Houston, 1990.

10. Sagues, A., Powers, R., Zayed, A., "Marine Environment Corrosion of Epoxy-Coated Reinforcing Steel", in Corrosion of Reinforcement in Concrete, C. Page, K.Treadway and P. Bamforth, Eds., pp.539-549, Elsevier Appl. Sci., London-New York, 1990.

11. Sohanghpurwala, A. and Clear, K., "Effectiveness of Epoxy Coatings in Minimizing Corrosion of Reinforcing Steel in Concrete", Transportation Rsch. Board, 69th Annual Meeting, Paper Preprint No. 89-0432, Washington, Jan.7-1, 1990.

12. Aguilar, A., Sagues, A. and Powers, R. Corrosion Measurements of Reinforcing Steel in Partially Submerged Concrete Slabs, in Corrosion Rates of Steel in Concrete, N.Berke, Ed., STP 1065, ASTM, Philadelphia, 1990.

13. Makita, M., Mori, Y. and Katawaki, K., "Marine Corrosion Behavior of Reinforced Concrete Exposed at Tokyo Bay", in ACI Publication SP-65, Performance of Concrete in Marine Environments, p. 271, V.Malhotra, Ed., American Concrete Institute, Detroit, 1980.

14. Rendell, F. and Miller, W., "Macrocell Corrosion of Reinforcement in Marine Structures", in Corrosion of Reinforcement in Concrete, C. Page, K. Treadway and P. Bamforth, Eds., pp.167-177, Elsevier Appl. Sci., London-New York, 1990.

15. Leidheiser, H., "Mechanisms of De-adhesion of Organic Coatings from Metal Surfaces", in Polymeric Materials for Corrosion Control, ACS Symp. Series 322, p.124, R. Dickie and F. Floyd, Eds., American Chemical Society, Washington, 1986.

16. Sagues, A. and Powers, R., to be published.

17. Guidelines for Inspection and Acceptance of Epoxy-Coated Reinforcing Bars at the Job Site, 1st. Ed., Concrete Reinforcing Steel Institute, Schaumburg, Illinois, 1986.

18. Millard, S. G., Durability Performance of Slender Reinforced Coastal Defense Units, in Concrete in Marine Environment, p.339, V. Malhotra, Ed., ACI SP-109, American Concrete Institute, Detroit, 1988.

19. Millard, S. G., Ghassemi, M., Bungey, J. and Jafar, M., "Assessing the Electrical Resistivity of Concrete Structures for Corrosion Durability Studies", in Corrosion of Reinforcement in Concrete, C. Page, K. Treadway and P. Bamforth, Eds., p.303, Elsevier Appl. Sci., London-New York, 1990.

20. Browne, R., "Mechanisms of Corrosion of Steel in Concrete in Relation to Design, Inspection and Repair of Offshore and Coastal structures", in Performance of Concrete in Marine Environment, Publication SP-65, American Concrete Institute, Detroit, 1980.

21. Monfore, G., "The Electrical Resistivity of Concrete", Journal of the PCA Research and Development Laboratories, May 1968, p.35.

22. Tuutti, K., Corrosion of Steel in Concrete, Swedish Cement and Concrete Research Institute, 1982.

23. Kaesche, H., "Metallic Corrosion", NACE, Houston, 1985.

24. Schwenk, W., Corr. Sci., Vol 23, p. 871, 1983.

25. Zayed, A. and Sagues, A., Corr. Sci., Vol. 30, p. 1025, 1990.

26. Andrade, C., Cruz-Alonso, M. and Gonzalez, J., "An Initial Effort to Use Corrosion Rate Measurements for Estimating Rebar Durability", in Corrosion Rates of Steel in Concrete, ASTM STP 1065, N. Berke, V. Chaker and D. Whiting, Eds., p.29, ASTM, Philadelphia, 1990.

27. Clear, K., Measuring Rate of Corrosion of Steel in Field Concrete Structures, TRB 68th Annual Meeting, January 22-26, 1989, Paper Preprint No. 88-0324.

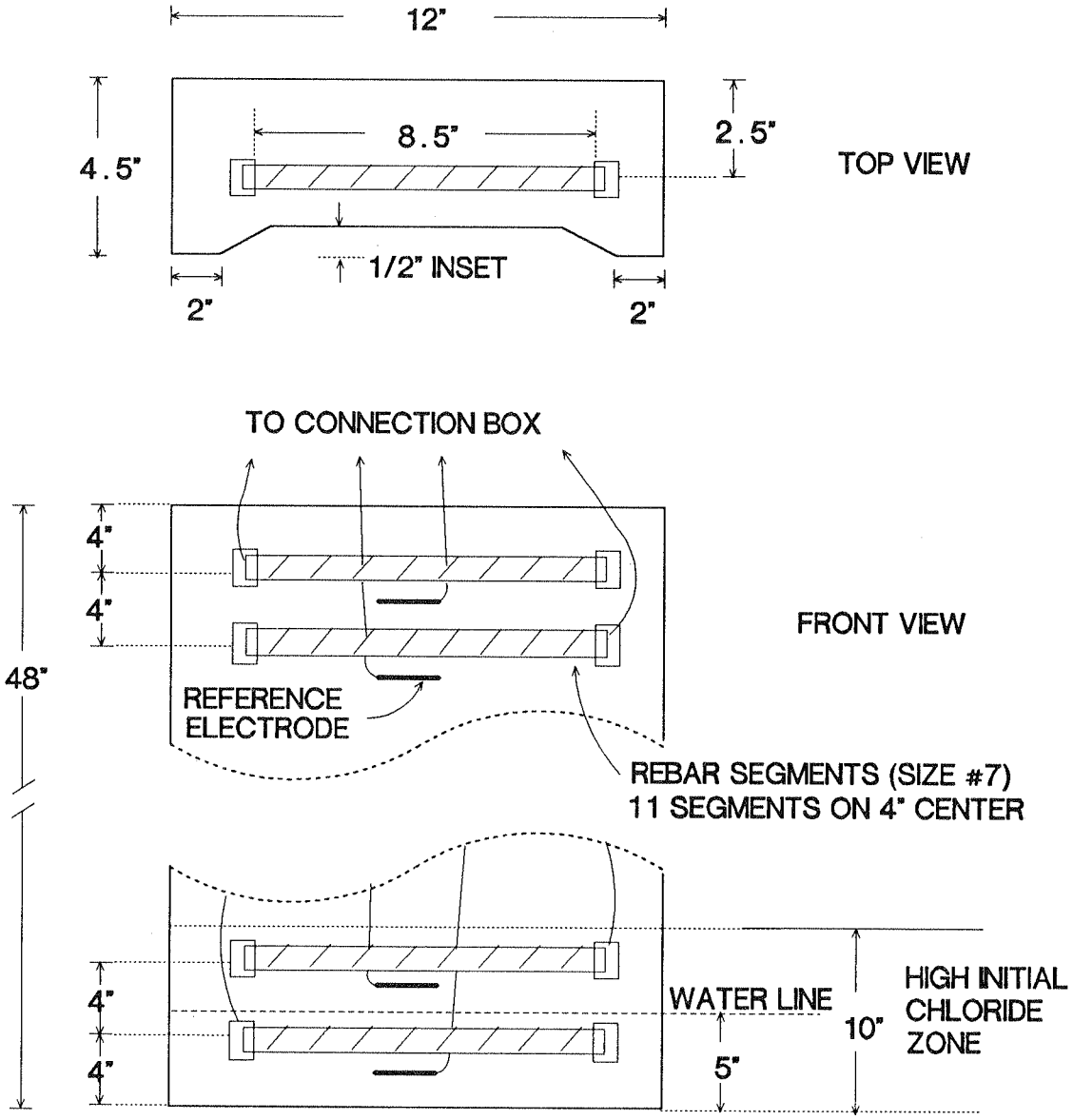

Figure 1 - Sketch of the laboratory column configuration (1 inch=2.54 cm.)

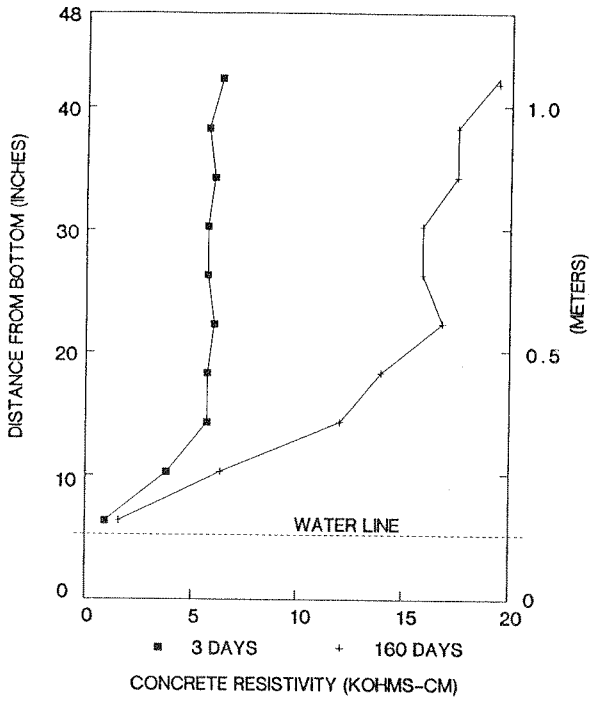

Figure 2 - Concrete resistivity as a function of position in column No.1, at the beginning of the test and after 160 days.

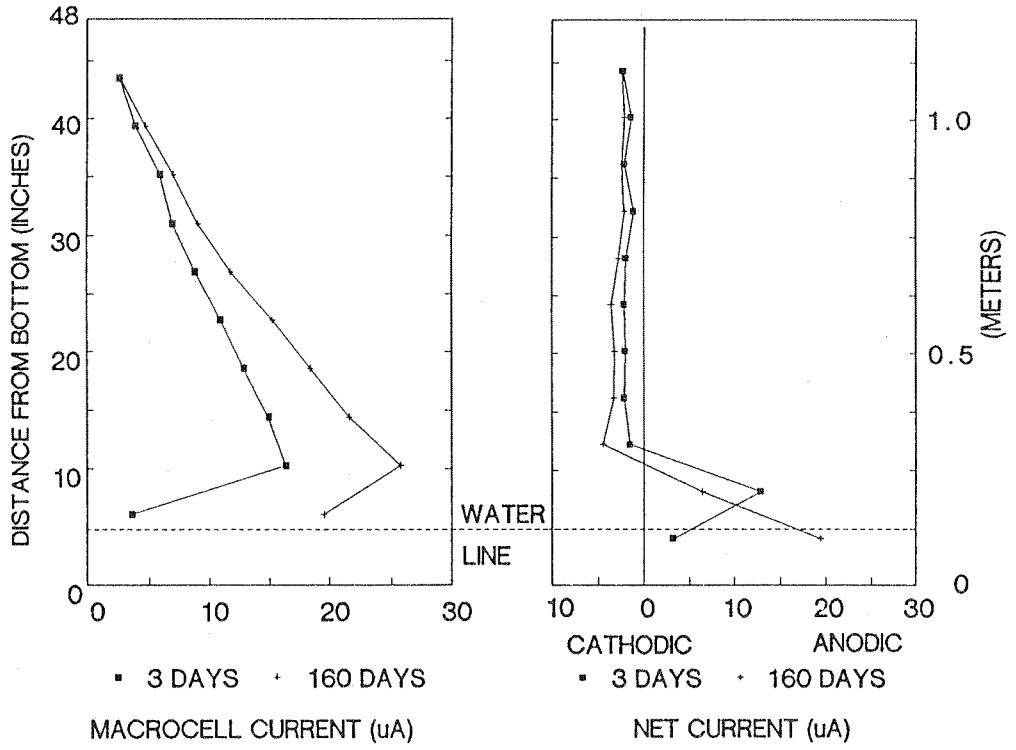

Figure 3 - Left side: Macrocell current measured at each of the 10 switches in column No. 1, shown as a function of the switch position, at the beginning of the test and after 160 days.

Right side: Current associated with each rebar segment in column No. 1, shown as a function of the segment position, at the beginning of the test and after 160 days.

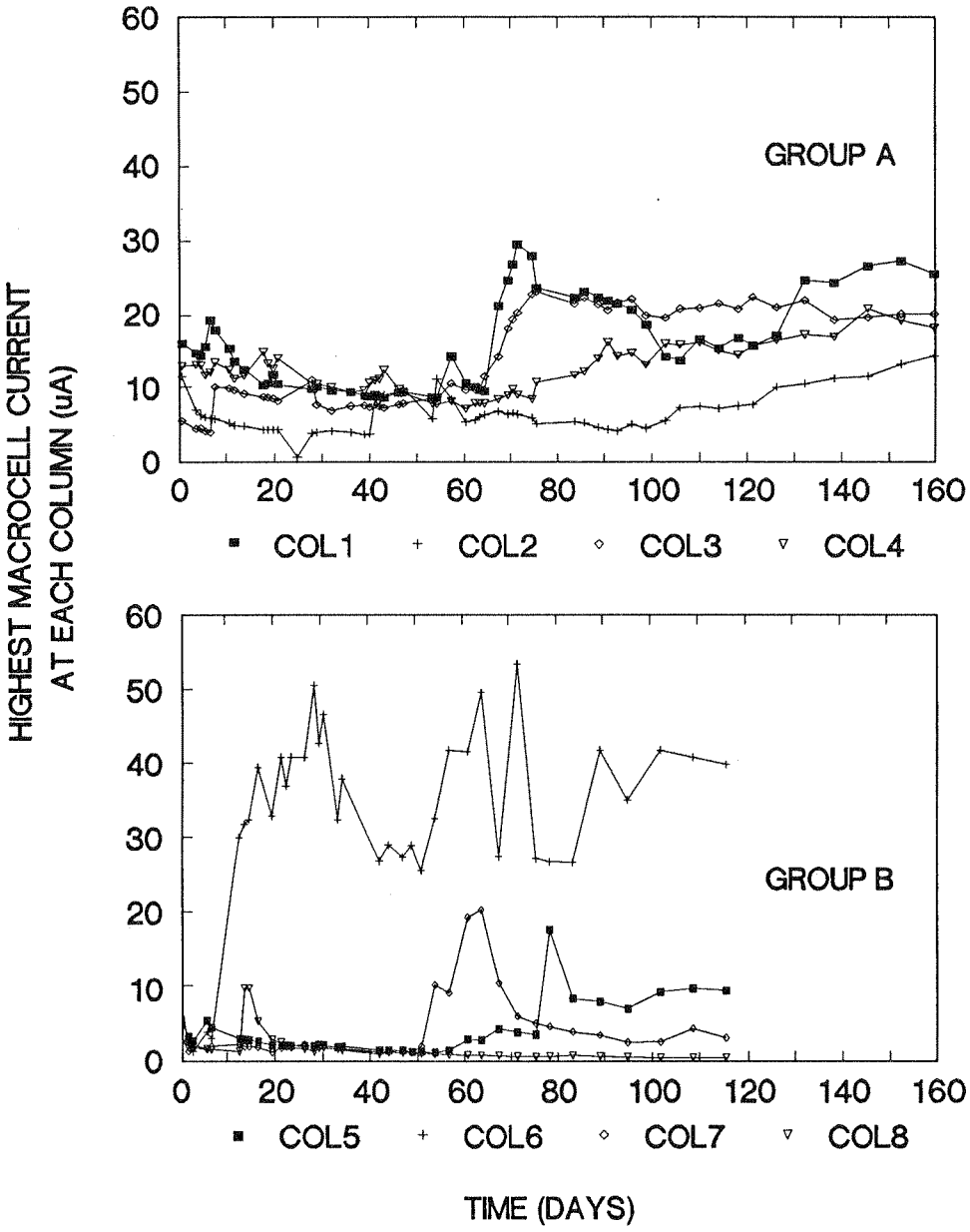

Figure 4 - Highest macrocell current (usually observed at switch #9, 10 inches from bottom) of each column as a function of exposure time. Group B was started later, so accumulated exposure times have been shorter.

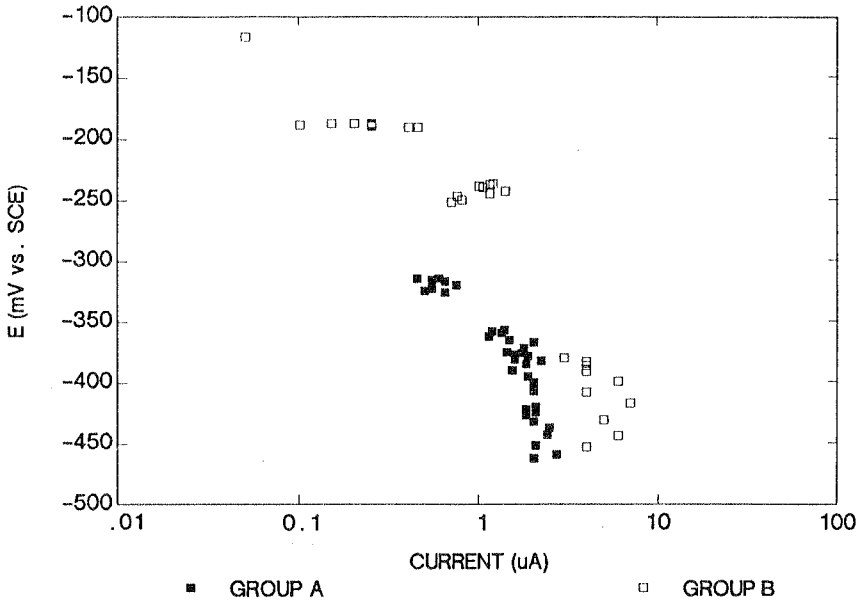

Figure 5 - Potential vs. current associated with each cathodic rebar segment for all test columns. The data corresponding to each column tend to lay within a small potential range, indirectly responding to the extent of anodic action of the column. The results for all columns within each group delineate a cathodic polarization curve. The point for the highest potential in group B shows the upper limit of cathodic current for that column; other segments in that columns had currents too small to be detected.

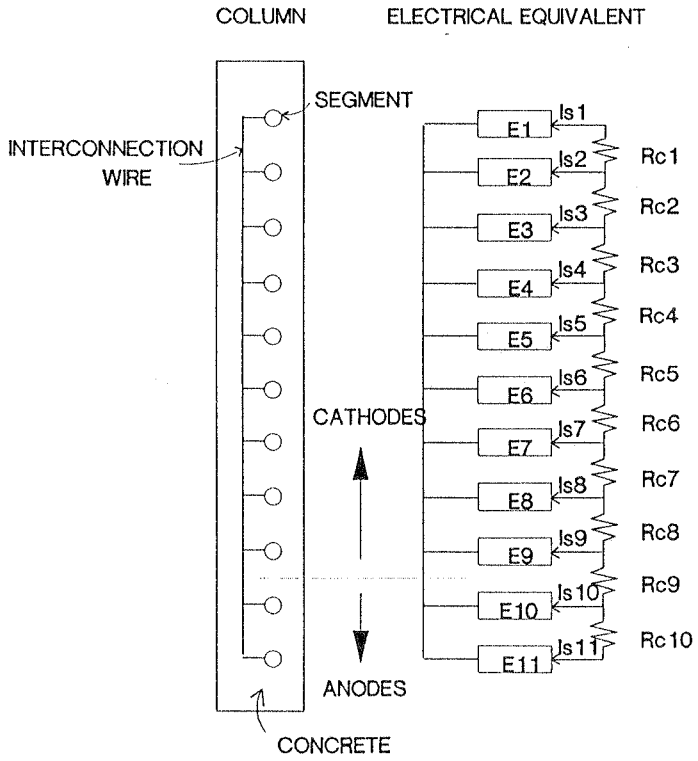

Figure 6 - Schematic of test column and electrical equivalent.

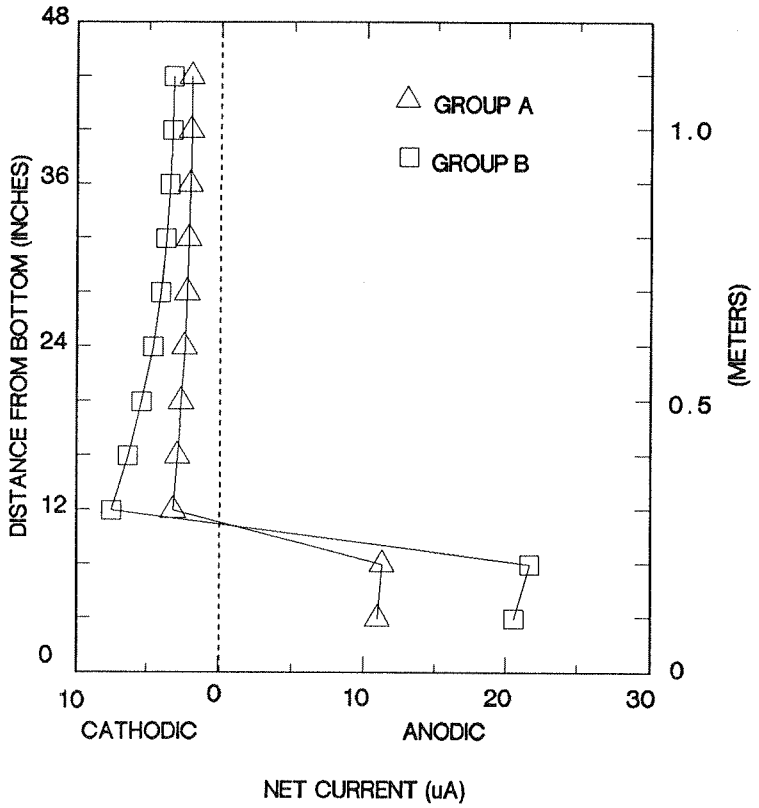

Figure 7 - Model predictions based on the assumed polarization parameters and concrete resistivity distribution for a laboratory column in each group (see text).

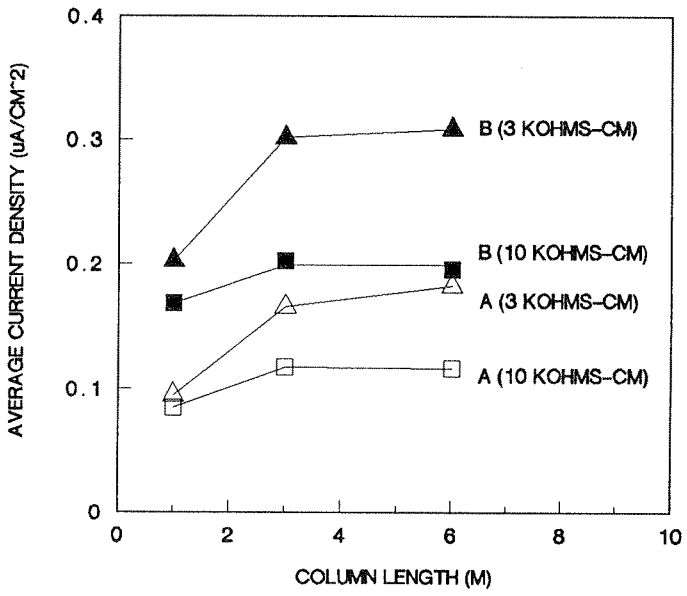

Figure 8 - Predicted average current densities at the upper of the two anodes for columns of uniform resistivity and various heights, where the rebar has the polarization characteristics assumed for column groups A and B. The steel-to-concrete proportion assumed is typical of the application of interest. (Note that the current density was calculated as an average over the entire bar segment, including both coated surface and bare metal spots.)